Journal of Alloys and Compounds 504 (2010) 16–21

Contents lists available at ScienceDirect

Journal of Alloys and Compounds

journal homepage: www.elsevier.com/locate/jallcom

Physical properties of $Zr_{50}Cu_{40-x}Al_{10}Pd_x$ bulk glassy alloys

M. Wencka[a,1], M. Jagodič[b], A. Gradišek[a], A. Kocjan[a], Z. Jagličić[b], P.J. McGuiness[a], T. Apih[a], Y. Yokoyama[c], J. Dolinšek[a,*]

[a] J. Stefan Institute, University of Ljubljana, Jamova 39, SI-1000 Ljubljana, Slovenia
[b] Institute of Mathematics, Physics and Mechanics, University of Ljubljana, Jadranska 19, SI-1000 Ljubljana, Slovenia
[c] Institute for Materials Research, Tohoku University, Katahira 2-1-1, Aobaku, Sendai 980-8577, Japan

ARTICLE INFO

Article history:
Received 30 April 2010
Received in revised form 9 May 2010
Accepted 14 May 2010
Available online 1 June 2010

Keywords:
Metallic glasses
Physical properties

ABSTRACT

It was shown recently (Yokoyama et al. [9]) that the addition of a small amount of Pd to the $Zr_{50}Cu_{40}Al_{10}$ bulk glassy alloy (BGA) has a beneficial effect on fatigue-strength enhancement, where the composition $Zr_{50}Cu_{37}Al_{10}Pd_3$ behaved in a resonant-like way by showing the highest fatigue limit of 1050 MPa and the minimum Vickers hardness. We performed a study of the magnetic properties, the specific heat, the electrical resistivity and the hydrogen-diffusion constant for a series of compositions $Zr_{50}Cu_{40-x}Al_{10}Pd_x$ (x = 0–7 at.%), in order to determine their physical properties and to check for the influence of the Pd content on these properties. The $Zr_{50}Cu_{40-x}Al_{10}Pd_x$ BGAs are nonmagnetic, conducting alloys, where the Pauli spin susceptibility of the conduction electrons is the only source of paramagnetism. The low-temperature specific heat indicates an enhancement of the conduction-electron effective mass m^* below 5 K, suggesting that the $Zr_{50}Cu_{40-x}Al_{10}Pd_x$ BGAs are not free-electron-like compounds. The electrical resistivities of the $Zr_{50}Cu_{40-x}Al_{10}Pd_x$ BGAs amount to about 200 μΩ cm and show a small, negative temperature coefficient (NTC) with an increase from 300 to 2 K of 4%. The hydrogen self-diffusion constant D in hydrogen-loaded samples shows classical over-barrier-hopping temperature dependence and is of comparable magnitude to the related icosahedral and amorphous $Zr_{69.5}Cu_{12}Ni_{11}Al_{7.5}$ hydrogen-storage alloys. No correlation between the investigated physical parameters and the Pd content of the samples could be observed.

1. Introduction

Bulk glassy alloys (BGAs) are amorphous, multi-component alloys of three or more chemical elements [1]. Examples include the ternary Co–Fe–B, the quaternary Zr–Cu–Ni–Al and the pentary Zr–Ti–Cu–Ni–Be. The best glass-forming ability is observed in systems with an atomic-radius mismatch between the elements of greater than 12%, leading to a higher packing density. BGAs show superior mechanical properties: (i) high strength (twice that of stainless steel, but lighter), (ii) hardness (for surface coating applications), (iii) toughness (more fracture resistant than ceramics) and (iv) elasticity (high yield strength). On the local scale of nearest neighbors, BGAs show short-range atomic order [2,3], where the atoms in the first coordination shell preferably form an icosahedron, resembling icosahedral quasicrystals. Other types of short-range clusters, such as trigonal prisms in B–Fe-based metallic glasses, are abundant as well.

Due to their unique combination of mechanical properties, BGAs exhibit great potential for industrial application. Here, the fatigue features play an important role. Since BGAs exhibit little plastic tensile elongation and no work-hardening phenomena, their fatigue features are different from those of ordinary crystalline materials. In crystalline plastic alloys, superior plasticity is provided by systematically moving the dislocations. In BGAs, there are no operable dislocations and the deformation mechanism is characterized by a unique, adiabatic shear-band operation [4], so that one-slip movement brings about a final fracture with little uniform plastic deformation. The lack of any uniform deformability of BGAs is considered as a limiting factor for the toughness [5].

Among the known BGAs, the Zr–Cu–Al alloy with the composition $Zr_{50}Cu_{40}Al_{10}$, close to the ternary eutectic point, was shown to exhibit a high glass-forming ability and superior mechanical properties [6–15]. In order to enhance the fatigue strength of the $Zr_{50}Cu_{40}Al_{10}$ BGA, the addition of a small amount of a fourth element (Pd, Ag, Pt and Au) was attempted [9]. It was observed that the element Pd has a particularly beneficial effect on

* Corresponding author at: J. Stefan Institute, University of Ljubljana, Department of Solid State Physics, Jamova 39, SI-1000 Ljubljana, Slovenia.
Tel.: +386 1 4773 740; fax: +386 1 4773 191.
E-mail address: jani.dolinsek@ijs.si (J. Dolinšek).
[1] On leave from the Institute of Molecular Physics, Polish Academy of Sciences, Smoluchowskiego 17, 60-179 Poznań, Poland.

0925-8388/$ – see front matter © 2010 Elsevier B.V. All rights reserved.
doi:10.1016/j.jallcom.2010.05.092

Table 1
Diamagnetic core susceptibility χ_{dia} calculated from literature tables [20] and the susceptibility $\chi = M/H$ obtained from the $M(H)$ curves at $T = 5$ K of the $Zr_{50}Cu_{40-x}Al_{10}Pd_x$ ($x = 0$, 1, 2, 3, 5 and 7 at.%) samples.

Sample	Abbreviation	Molar mass (g/mol)	χ_{dia} (emu/mol)	χ (emu/mol)
$Zr_{50}Cu_{40}Al_{10}$	Pd-0	73.73	-9.60×10^{-6}	8.2×10^{-5}
$Zr_{50}Cu_{39}Al_{10}Pd_1$	Pd-1	74.16	-9.53×10^{-6}	7.8×10^{-5}
$Zr_{50}Cu_{38}Al_{10}Pd_2$	Pd-2	74.59	-9.46×10^{-6}	7.8×10^{-5}
$Zr_{50}Cu_{37}Al_{10}Pd_3$	Pd-3	75.01	-9.39×10^{-6}	8.2×10^{-5}
$Zr_{50}Cu_{35}Al_{10}Pd_5$	Pd-5	75.87	-9.25×10^{-6}	8.5×10^{-5}
$Zr_{50}Cu_{33}Al_{10}Pd_7$	Pd-7	76.73	-9.11×10^{-6}	7.6×10^{-5}

the fatigue-strength enhancement, by promoting glass-structure expansion that can be recognized from the volume shrinkage after structural relaxation at high temperature. A linear relationship between the fatigue limit and the volume change was observed in the series $Zr_{50}Cu_{40-x}Al_{10}Pd_x$ ($x = 0$–7 at.%) BGAs. The composition $Zr_{50}Cu_{37}Al_{10}Pd_3$ behaved in a resonant-like way by showing the highest fatigue limit of 1050 MPa, the minimum Vickers hardness and the largest volume change of about 0.5% from the as-cast state to the fully relaxed state. The large volume change indicates the existence of a thermally unstable volume (also termed the excessive free volume) below the glassy temperature T_g in the amorphous structure, when we assume that the amorphous structure is composed of clusters and voids. Thermally unstable voids are very likely effective in relaxing localized stress, because the atoms surrounding the voids move more easily than others. This superior ability of the stress relaxation has an advantageous impact on the fracture and fatigue properties.

The origin of the exceptional fatigue properties of the particular composition $Zr_{50}Cu_{37}Al_{10}Pd_3$ deserves further attention. In this paper we present an investigation of the physical properties of the $Zr_{50}Cu_{40-x}Al_{10}Pd_x$ ($x = 0$–7 at.%) series, including the magnetic properties, the specific heat, the electrical resistivity and an NMR determination of the hydrogen-diffusion constant in hydrogen-loaded samples using the same material as that investigated for the fatigue and other mechanical properties [9]. The aim of our investigation is twofold: (i) to determine the physical properties of this technologically important BGA material and (ii) to see whether the systematic variation of the Pd content also introduces systematic variation of the investigated physical properties of the $Zr_{50}Cu_{40-x}Al_{10}Pd_x$ BGAs, which is the case for their mechanical properties.

2. Materials characterization

The preparation of the $Zr_{50}Cu_{40-x}Al_{10}Pd_x$ ($x = 0$, 1, 2, 3, 5 and 7 at.%) materials has been described in detail in a previous publication [9]. Special care was taken to maintain a low oxygen concentration using a special Zr crystal rod (<0.05 at.% oxygen), since oxygen in Zr-based amorphous alloys significantly affects the glass-forming ability by promoting crystallization [16–18]. The cast rods of 8-mm diameter and 60-mm length were prepared using the tilt-cast technique [19], which is effective in eliminating the crystalline inclusions that act as crack-initiation sites and enhance the crack propagation during the fatigue test. For the physical measurements, rectangular rods of 2 mm × 2 mm × 8 mm were cut from the parent ingots, except for the specific heat, where cubes with 2-mm edges were used. Further characterization of the samples using X-ray, TEM, SEM and mechanical tests was given in a previous paper [9]. In the following, we denote the samples according to their palladium content, as Pd-x with $x = 1$–7 (e.g., Pd-3 standing for $Zr_{50}Cu_{37}Al_{10}Pd_3$ and Pd-0 for $Zr_{50}Cu_{40}Al_{10}$). The denotations are also given in Table 1. For the NMR diffusion measurements, small parts of the samples were crushed into powder in order to ensure homogeneous penetration of the radiofrequency electromagnetic field in the material due to the skin effect.

3. Magnetic properties

The temperature-dependent magnetic susceptibility, $\chi(T)$, and the magnetization as a function of the magnetic field, $M(H)$, were investigated using a Quantum Design MPMS XL-5 SQUID magnetometer, equipped with a 50 kOe magnet. The susceptibilities $\chi(T)$ of all the samples, measured in the temperature interval between 300 and 2 K in a magnetic field of 1 kOe, are displayed in Fig. 1a. The susceptibilities are almost temperature-independent, showing a tiny increase of about 1% upon heating from 2 to 300 K. This is more evident from the inset in Fig. 1a, where the susceptibilities are displayed on an expanded vertical scale. Random order of the susceptibilities with respect to the Pd concentration also demonstrates that no systematic correlation between the magnitude of $\chi(T)$ and the Pd content of the samples can be inferred.

The $M(H)$ curves at $T = 5$ K are displayed in Fig. 1b. For all samples, the $M(H)$ dependence is linear positive paramagnetic within

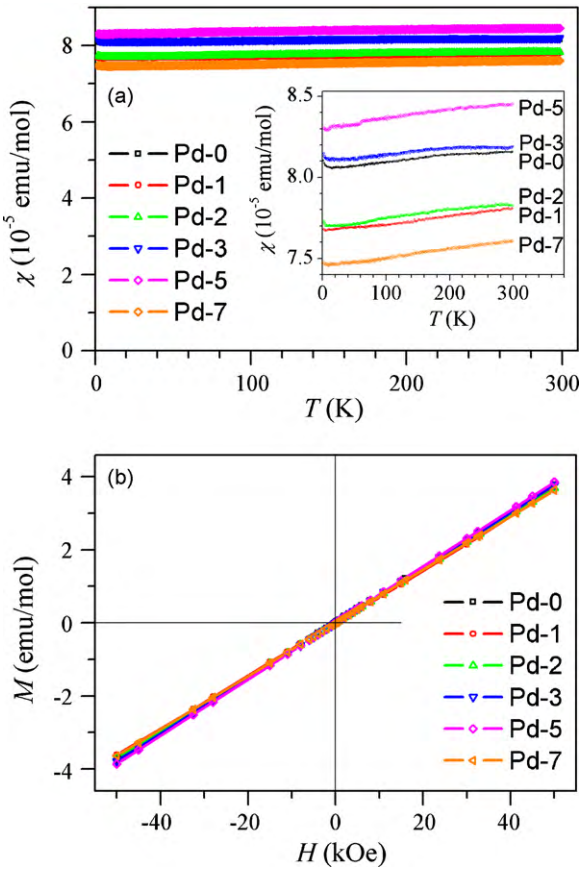

Fig. 1. (a) Temperature-dependent magnetic susceptibility $\chi = M/H$ of the $Zr_{50}Cu_{40-x}Al_{10}Pd_x$ ($x = 0$, 1, 2, 3, 5 and 7 at.%) samples, measured in a magnetic field of 1 kOe. The samples are labeled according to their Pd concentration as Pd-0 to Pd-7. The inset shows the susceptibilities on an expanded vertical scale. (b) Magnetization M as a function of the magnetic field H at $T = 5$ K in the field range ±50 kOe.

the investigated field range of ±50 kOe. There is no pronounced difference between the $M(H)$ lines of different samples, which are the same within the experimental precision.

In order to determine the type of magnetic susceptibility, we calculated the diamagnetic core susceptibility χ_{dia} from literature tables [20]. All the χ_{dia} values are close to -1×10^{-5} emu/mol (Table 1). In Table 1, the magnetic susceptibility $\chi = M/H$ values obtained from the $M(H)$ curves at $T = 5$ K of Fig. 1b are also given (practically identical values are obtained from the $\chi(T)$ curves displayed in Fig. 1a). The χ values are in the range $[7.6, 8.2]\times10^{-5}$ emu/mol, and are thus of a comparable magnitude to the diamagnetic core susceptibility. The same order of magnitude of χ and χ_{dia} and the almost temperature-independent $\chi(T)$ classify the susceptibility of the investigated Pd-0 to Pd-7 samples to the Pauli spin susceptibility of the conduction electrons. The tiny increase of $\chi(T)$ with increasing temperature by about 1% between 2 and 300 K can be attributed to the lowest-order temperature corrections of the Pauli spin susceptibility (being of the type $aT^2 + bT^4$), emerging from the temperature dependence of the chemical potential μ and the variation of the electronic density of states (DOS) with an energy in the vicinity of the Fermi energy ε_F. Since the Pauli spin susceptibility is the only source of paramagnetism in the $Zr_{50}Cu_{40-x}Al_{10}Pd_x$ BGAs, these alloys can be classified among the nonmagnetic conducting alloys.

4. Specific heat

The low-temperature specific heat $C(T)$ is related to the electronic DOS at ε_F and the Debye temperature θ_D. The electronic specific heat depends linearly on the temperature, $C_{el}(T) = \gamma T$, with the electronic specific heat coefficient $\gamma = (\pi^2/3)k_B^2 g(\varepsilon_F)$, where $g(\varepsilon_F)$ is the DOS at ε_F. At low temperatures below about 10 K, the lattice specific heat can usually be well approximated by the Debye model and is expressed as a function of temperature in the form $C_{latt}(T) = \alpha T^3$. The lattice specific heat coefficient α is related to the Debye temperature via the relation $\theta_D = (12\pi^4 R/5\alpha)^{1/3}$, where R is the gas constant. The total specific heat at low temperatures can be written as

$$C = \gamma T + \alpha T^3. \quad (1)$$

In order to extract γ and α, Eq. (1) is usually rewritten in the form $C/T = \gamma + \alpha T^2$. Plotting the low-temperature C/T data versus T^2 yields a straight line with the intercept γ and the slope α.

Specific heat measurements were performed in the temperature range between 2 and 300 K using a Quantum Design Physical Property Measurement System (PPMS) that employs a thermal-relaxation calorimeter. The low-temperature molar specific heats of all the investigated $Zr_{50}Cu_{40-x}Al_{10}Pd_x$ samples in the temperature range between 2 and 14 K are displayed in Fig. 2a in a C/T versus T^2 plot. The data analysis of the Pd-0 sample that is representative of all the samples is shown in Fig. 2b. Between 14 and 5 K, the C/T versus T^2 data fall on a straight line, whereas in the low-temperature regime between 5 and 2 K, a slight change of slope is noticed and the C/T values are enhanced with respect to the extrapolated prediction from the upper temperature range (inset in Fig. 2b). Such a behavior usually indicates an enhancement of the electronic specific heat coefficient γ at low temperatures due to electron–electron interactions that result in an enhancement of the conduction-electron effective mass m^*. This suggests that the $Zr_{50}Cu_{40-x}Al_{10}Pd_x$ BGAs are not free-electron-like compounds. The solid line in Fig. 2b is the fit of the data in the upper temperature range 14–5 K with the equation $C/T = \gamma + \alpha T^2$, and the γ and θ_D values are given in Table 2. The experimental γ_{exp} value, obtained by extrapolating the low-temperature 2–5 K experimental data to zero temperature (see inset in Fig. 2b) that gives the enhanced γ value is presented in

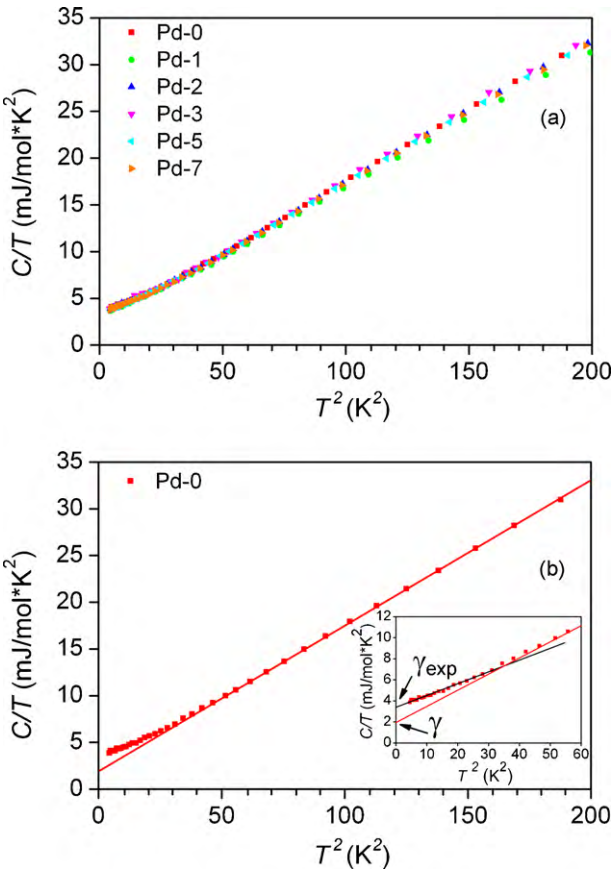

Fig. 2. (a) Low-temperature specific heat of the $Zr_{50}Cu_{40-x}Al_{10}Pd_x$ ($x = 0$, 1, 2, 3, 5 and 7 at.%) samples in the temperature range between 2 and 14 K displayed in a C/T versus T^2 plot. The samples are labeled according to their Pd concentration as Pd-0 to Pd-7. (b) Data analysis of the Pd-0 sample. Solid line is the fit in the upper temperature range 14–5 K with the equation $C/T = \gamma + \alpha T^2$, where γ represents the $T = 0$ intercept on the vertical axis. The inset shows the low-temperature data. The online-red line is a continuation of the fit from the 14–5 K range, giving the intercept γ, whereas the online-black line is the fit of the 2–5 K data that gives the intercept γ_{exp}. Both intercepts are marked by arrows. (For interpretation of the references to color in this figure legend, the reader is referred to the web version of the article.)

Table 2 as well. The same analysis was performed for all the samples and the parameter values are collected in Table 2. The γ, γ_{exp} and θ_D values of the investigated samples are scattered randomly around the mean values $\bar{\gamma} = 2.08 \pm 0.08$ mJ/mol K^2, $\bar{\gamma}_{exp} = 3.36 \pm 0.08$ mJ/mol K^2 and $\theta_D = 235 \pm 5$ K. This scatter is small enough to represent the experimental error and no systematic correlation of the coefficients to the Pd content of the samples can be claimed. The specific heat properties of the investigated $Zr_{50}Cu_{40-x}Al_{10}Pd_x$ series are thus the same within the experimental precision, regardless of the Pd content.

Table 2
Electronic specific heat coefficient γ and the Debye temperature θ_D of the investigated $Zr_{50}Cu_{40-x}Al_{10}Pd_x$ ($x = 0$, 1, 2, 3, 5 and 7 at.%) samples. The γ and θ_D values were obtained from the fit of the C/T versus T^2 data with the function $\gamma + \alpha T^2$ in the upper temperature range 14–5 K (solid line in Fig. 2b), whereas the γ_{exp} values were obtained by extrapolating the low-temperature 2–5 K experimental data to zero temperature (inset in Fig. 2b).

Sample	γ (mJ/mol·K^2)	γ_{exp} (mJ/mol·K^2)	θ_D (K)
Pd-0	2.16	3.44	233
Pd-1	2.02	3.14	246
Pd-2	2.10	3.43	233
Pd-3	2.08	3.42	232
Pd-5	2.00	3.35	233
Pd-7	2.12	3.39	234

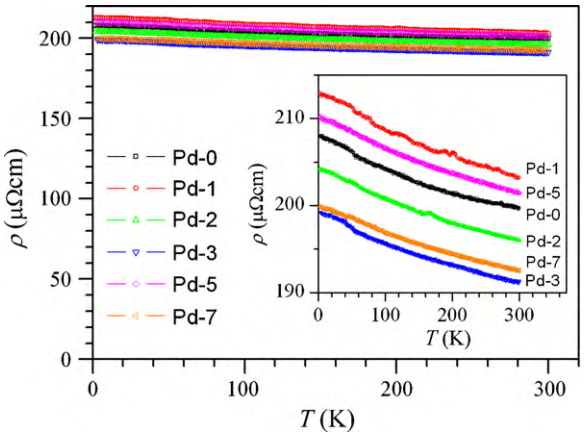

Fig. 3. Temperature-dependent electrical resistivity $\rho(T)$ of the $Zr_{50}Cu_{40-x}Al_{10}Pd_x$ (x = 0, 1, 2, 3, 5 and 7 at.%) samples. The samples are labeled according to their Pd concentration as Pd-0 to Pd-7. The inset shows the resistivities on an expanded vertical scale.

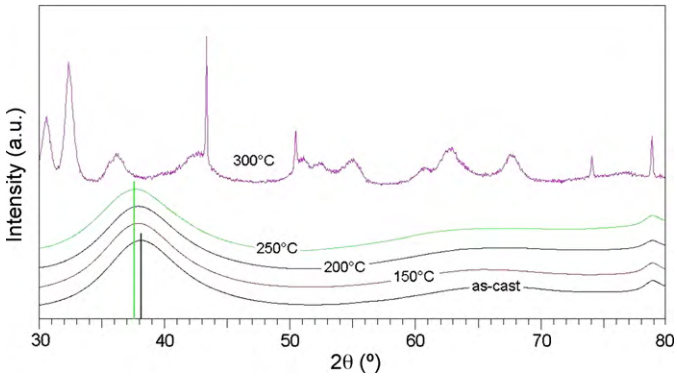

Fig. 4. X-ray diffraction spectra of the $Zr_{50}Cu_{33}Al_{10}Pd_7$ material hydrogen-loaded from the gas phase at a set of different temperatures (as-cast material at room temperature, 150, 200, 250 and 300 °C) at a pressure of 4.5 MPa and a loading time of 1000 min. An increased hydrogen absorption rate at higher temperatures results in an increased shift of the X-ray peak due to the first coordination shell at the scattering angle $2\theta \approx 38°$ towards lower angles (marked by the vertical lines). Hydrogen loading at 300 °C resulted in partial crystallization of the material.

5. Electrical resistivity

The electrical resistivity was measured between 300 and 2 K using the standard four-terminal technique. The $\rho(T)$ data of the $Zr_{50}Cu_{40-x}Al_{10}Pd_x$ samples are displayed in the main panel of Fig. 3, whereas the inset shows the resistivities on an expanded vertical scale. The 300 K resistivity values are in the range 191–203 μΩ cm, and are thus within 5% of the average value $\bar{\rho}_{300K} = 196$ μΩ cm. Since the experimental error in the absolute resistivity values is of the same order, the resistivities of all $Zr_{50}Cu_{40-x}Al_{10}Pd_x$ samples should be considered as the same within the experimental precision. Random order of the resistivities with respect to the Pd concentration also demonstrates that there is no correlation between the resistivity values and the Pd content of the samples.

All the resistivities show a small, negative temperature coefficient (NTC), where the resistivity increase from 300 to 2 K upon cooling is by a factor $(\rho_{2K} - \rho_{300K})/\rho_{300K}$ = 4%. The NTC is again practically the same for all samples. The non-metallic NTC resistivity is reminiscent of icosahedral quasicrystals like *i*-Al–Cu–Fe [21], *i*-Al–Pd–Mn and *i*-Al–Pd–Re [22] that exhibit a pseudogap in the electronic DOS at ε_F, but the resistivity values of these compounds are much higher (the 300 K values are usually above 1000 μΩ cm), as compared to the $Zr_{50}Cu_{40-x}Al_{10}Pd_x$ samples. Other metallic systems exhibiting NTC resistivities with values comparable to those of the $Zr_{50}Cu_{40-x}Al_{10}Pd_x$ samples are alloys and compounds in which the electron mean-free-path l between the scattering events is small compared to the extension of the conduction-electron wave packet L_{wp}, in which case the electron propagation is non-Boltzmann (non-ballistic) and the resistivity exhibits a NTC [23]. The lack of translational periodicity in the amorphous structure of the $Zr_{50}Cu_{40-x}Al_{10}Pd_x$ BGAs implies that the relaxation time τ between scattering events is short, so that $l = v\tau$ (where v is the electron velocity) is small and the short mean-free-path limit $l < L_{wp}$ can easily be met. The short mean-free-path hypothesis thus offers a realistic explanation of the non-metallic NTC resistivity in the investigated $Zr_{50}Cu_{40-x}Al_{10}Pd_x$ series. A similar situation was recently found also in the $Al_{80}Cr_{15}Fe_5$ complex metallic alloy [24].

6. NMR determination of the hydrogen-diffusion constant in $Zr_{50}Cu_{40-x}Al_{10}Pd_x$

It was shown [9,12] that the introduction of hydrogen into the $Zr_{50}Cu_{40-x}Al_{10}Pd_x$ BGAs strongly affects their fatigue properties. Significant hardening on the fatigue-fractured surface was observed upon hydrogenation, where this hydrogen hardening may be considered as a substitution of the strain-aging effect. No crystallization could be observed on the fatigue-fractured surface region by X-ray diffraction and TEM observations, so that hydrogen increases the hardness of this BGA material, while keeping its glassy structure. Recently, the influence of hydrogen concentration on the fatigue-fractured surface was reported by nuclear reaction analysis, which used accelerated ^{15}N ions up to 6.385 MeV to determine the hydrogen enrichment near the surface [12]. By controlling the hydrogen content in the $Zr_{50}Cu_{40-x}Al_{10}Pd_x$ BGAs, a high fatigue limit over 1 GPa could be obtained for the composition $Zr_{50}Cu_{37}Al_{10}Pd_3$ [9].

Due to the advantageous influence of hydrogen on the fatigue properties of the $Zr_{50}Cu_{40-x}Al_{10}Pd_x$ BGAs, we attempted to determine whether the hydrogen in the amorphous structure is chemically bound to the metallic ions and hence statically distributed over the material or the hydrogen atoms can move throughout the amorphous structure and their spatial distribution is dynamic. To elucidate this question, we performed a measurement of the hydrogen self-diffusion constant D by ^1H NMR spectroscopy. Unlike the hydrogenated samples used in the fatigue-property measurements [9,12] that were charged electrolytically, our $Zr_{50}Cu_{40-x}Al_{10}Pd_x$ were hydrogen-loaded from the gas phase. The amount of absorbed hydrogen was monitored by determining the shift of the X-ray peak due to the first coordination shell at the angle $2\theta \approx 38°$ (Fig. 4) towards lower angles, as a consequence of the lattice expansion upon hydrogen absorption. The different Pd concentrations of the samples had quite a strong influence on the loading conditions. In order to load the samples with different Pd contents to the same hydrogen-to-metal (H/M) ratio (producing the same X-ray shifts), the loading conditions were varied between the samples by setting the hydriding temperature between 240 and 270 °C, the loading times between 500 and 2000 min and the pressure constant at 4.5 MPa. These values were predefined by a series of trial loading experiments. An example is shown in Fig. 4, where the hydrogen absorption in the sample with the largest Pd content (Pd-7) was fixed at various values using different temperatures (room temperature, 150, 200, 250 and 300 °C) at a pressure of 4.5 MPa and loading time of 1000 min. It is clear that the shift of the X-ray peak at $2\theta \approx 38°$ towards lower angles continuously increases with increasing temperature, showing that (i) hydrogen is stored in the bulk of the material and (ii) higher loading temperatures result in a higher hydrogen absorption rate. Hydrogen loading at 300 °C resulted in a partial crystallization of the mate-

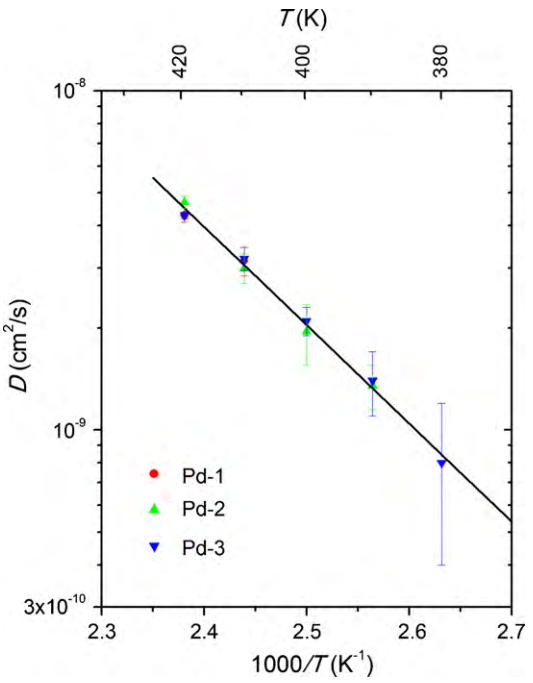

Fig. 5. Temperature-dependent hydrogen-diffusion constant D in the $Zr_{50}Cu_{40-x}Al_{10}Pd_x$ ($x>0$) samples (only the representative data of the Pd-1, Pd-2 and Pd-3 samples are shown). Solid line is the fit with $D = D_0 \exp(-E_a/k_BT)$ using the average activation energy of all samples $\bar{E}_a = 576$ meV.

rial (the amorphous X-ray pattern has disappeared and a set of discrete diffraction lines has appeared in the 300 °C spectrum in Fig. 4), which limited the highest loading temperature to 270 °C. Estimated from the final X-ray shifts, our $Zr_{50}Cu_{40-x}Al_{10}Pd_x$ samples with different Pd contents were all loaded to a very similar value $H/M \approx 0.2$.

The hydrogen-diffusion constant was determined from the diffusion-induced attenuation of the ^{1}H NMR spin-echo in a static fringe field (SFF) of a superconducting magnet [25]. The SFF method takes advantage of the ultra-high magnetic field gradients (typically up to 80 T/m) of the highly stable static fringe field of an NMR superconducting magnet, extending the sensitivity to molecular diffusion down to the extremely low values $D \geq 10^{-11}$ cm^2/s. The SFF diffusion experiments were in the past successfully applied to determine the temperature-dependent diffusion constant of the icosahedral and amorphous $Zr_{69.5}Cu_{12}Ni_{11}Al_{7.5}$ alloys [26–28]. The SFF experiments on the $Zr_{50}Cu_{40-x}Al_{10}Pd_x$ BGAs were conducted in a superconducting magnet with a center field of 9.39 T. The probe head was fine-positioned at one edge of the superconducting coil, where the proton resonance frequency amounted to $\nu(^1\text{H})$=200 MHz and the gradient was g = 68 T/m. The stimulated spin-echo pulse sequence was used. Other experimental details and the data analysis are identical to those described in the preceding papers [26–28].

The hydrogen-diffusion constant in the $Zr_{50}Cu_{40-x}Al_{10}Pd_x$ ($x>0$) samples was determined in the temperature interval between 380 and 420 K (Fig. 5), where the D values are within the range between 7×10^{-10} and 8×10^{-9} cm^2/s. The $D(T)$ data points fall on straight lines in the log D versus $1/T$ plot, indicating a simple classical (Arrhenius) over-barrier-hopping hydrogen diffusion with $D = D_0 \exp(-E_a/k_BT)$, where E_a is the activation energy. The $D(T)$ data of all the samples fall on the same line within an experimental precision of ~10% (in Fig. 5, only the representative data of the Pd-1, Pd-2 and Pd-3 samples are shown), so that no correlation of the diffusion constant to the Pd content of the samples can be claimed. The analysis yielded an average activation energy for all the samples of $\bar{E}_a = 576 \pm 15$ meV and a diffusion prefactor $D_0 = 3.6 \pm 1.5 \times 10^{-2}$ cm^2/s. Compared to the activation energies of the previously investigated icosahedral and amorphous $Zr_{69.5}Cu_{12}Ni_{11}Al_{7.5}$ alloys [26–28], the $\bar{E}_a$ value of $Zr_{50}Cu_{40-x}Al_{10}Pd_x$ BGAs is about 20% higher, which very likely originates from their different chemical compositions. The substantial hydrogen-diffusion constant in the $Zr_{50}Cu_{40-x}Al_{10}Pd_x$ BGAs shows that hydrogen is not chemically bound to the metal atoms, but moves relatively freely through the amorphous structure.

7. Summary and conclusions

The $Zr_{50}Cu_{40}Al_{10}$ BGA exhibits a high glass-forming ability and superior mechanical properties. The addition of a small amount of Pd has a beneficial effect on the fatigue-strength enhancement, where the composition $Zr_{50}Cu_{37}Al_{10}Pd_3$ behaves in a resonant-like way by showing the highest fatigue limit of 1050 MPa, the minimum Vickers hardness and the largest volume change of about 0.5% from the as-cast state to the fully relaxed state. In order to determine the physical properties of this technologically important BGA material, we studied the magnetic properties, the specific heat, the electrical resistivity and the hydrogen-diffusion constant in a series of compositions $Zr_{50}Cu_{40-x}Al_{10}Pd_x$ (x = 0–7 at.%). The results can be summarized as follows.

(1) The $Zr_{50}Cu_{40-x}Al_{10}Pd_x$ BGAs are nonmagnetic conducting alloys, where the Pauli spin susceptibility of the conduction electrons is the only source of paramagnetism. No systematic correlation between the magnitude of the magnetization or susceptibility to the Pd content of the samples could be observed.
(2) The low-temperature specific heat indicates an enhancement of the electronic specific heat coefficient γ at temperatures below 5 K, compatible with the enhancement of the conduction-electron effective mass m^* due to electron–electron interactions. This suggests that the $Zr_{50}Cu_{40-x}Al_{10}Pd_x$ BGAs are not free-electron-like compounds. No systematic correlation of the specific heat coefficients to the Pd content of the samples can be claimed within the experimental precision.
(3) The electrical resistivities of the $Zr_{50}Cu_{40-x}Al_{10}Pd_x$ BGAs at room temperature amount to about 200 μΩ cm and show a small NTC with the increase from 300 to 2 K of 4%. The resistivities of all the samples can be considered as the same within the experimental precision, and there exists no correlation between the resistivity values and the Pd content of the samples. The non-metallic NTC resistivity of the metallic $Zr_{50}Cu_{40-x}Al_{10}Pd_x$ BGAs very likely originates from the non-ballistic propagation of the charge carriers due to their short mean-free-path between the scattering events in the amorphous structure.
(4) Since the introduction of hydrogen into the $Zr_{50}Cu_{40-x}Al_{10}Pd_x$ BGAs has an advantageous influence on their fatigue properties, we have performed measurements of the hydrogen self-diffusion constant D using ^{1}H NMR spectroscopy. Within the temperature interval 380–420 K, the D values are between 7×10^{-10} and 8×10^{-9} cm^2/s and show a classical (Arrhenius) over-barrier-hopping temperature dependence. No correlation between the diffusion constant and the Pd content of the samples could be observed within the experimental precision. The average hopping activation energy of all the samples amounts to $\bar{E}_a = 576 \pm 15$ meV. The hydrogen-diffusion constant of the $Zr_{50}Cu_{40-x}Al_{10}Pd_x$ BGAs is of comparable magnitude to that of the related icosahedral and amorphous $Zr_{69.5}Cu_{12}Ni_{11}Al_{7.5}$ alloys.

(5) The resonant character of the mechanical properties of the particular composition $Zr_{50}Cu_{37}Al_{10}Pd_3$ is not reflected in the investigated physical properties of the $Zr_{50}Cu_{40-x}Al_{10}Pd_x$ (x = 0–7 at.%) series, which do not depend on the Pd content within the experimental precision.

References

[1] See, for a review: M. Telford, Materials Today, Elsevier, Kidlington, UK, 2004, p. 36, March 2004 issue.
[2] W.K. Luo, H.W. Sheng, F.M. Alamgir, J.M. Bai, J.H. He, E. Ma, Phys. Rev. Lett. 92 (2004) 145502.
[3] Y.T. Shen, T.H. Kim, A.K. Gangopadhyay, K.F. Kelton, Phys. Rev. Lett. 102 (2009) 057801.
[4] H.S. Chen, T.T. Wang, J. Appl. Phys. 41 (1970) 5338.
[5] C.C. Hays, C.P. Kim, W.L. Johnson, Phys. Rev. Lett. 84 (2000) 2901.
[6] M. Ishida, T. Uehara, T. Arai, H. Takeda, T. Yamaguchi, T. Tniguchi, T. Katsumi, M. Kobayashi, H. Ofune, Intermetallics 10 (2002) 1259.
[7] Y. Yokoyama, K. Fukaura, A. Inoue, Mater. Trans. 45 (2004) 1672.
[8] Y. Yokoyama, Y. Akeno, T. Yamasaki, P.K. Liaw, R.A. Buchanan, A. Inoue, Mater. Trans. 46 (2005) 2755.
[9] Y. Yokoyama, P.K. Liaw, M. Nishijima, K. Hiraga, R.A. Buchanan, A. Inoue, Mater. Trans. 47 (2006) 1286.
[10] Y. Yokoyama, T. Yamasaki, P.K. Liaw, A. Inoue, Mater. Trans. 48 (2007) 1846.
[11] Y. Yokoyama, A. Inoue, Mater. Trans. 48 (2007) 1282.
[12] Y. Yokoyama, M. Wilde, K. Fukutani, A. Inoue, Mater. Trans. 48 (2007) 1261.
[13] Y. Yokoyama, K. Fujita, A.R. Yavari, A. Inoue, Philos. Mag. Lett. 89 (2009) 322.
[14] Y. Yokoyama, T. Yamasaki, P.K. Liaw, A. Inoue, Acta Mater. 56 (2008) 6097.
[15] Y. Yokoyama, T. Ishikawa, J.T. Okada, Y. Watanabe, S. Nanao, A. Inoue, J. Non-Cryst. Solids 355 (2009) 317.
[16] L. Johnson, Mater. Sci. Forum 225–227 (1996) 35.
[17] X.H. Lin, W.L. Johnson, W.K. Rhim, Mater. Trans. JIM 38 (1997) 473.
[18] A. Kubler, J. Eckert, A. Gebert, L. Schultz, J. Appl. Phys. 83 (1998) 3438.
[19] Y. Yokoyama, A. Inoue, K. Fukaura, Mater. Trans. 43 (2002) 2316.
[20] P.W. Selwood, Magnetochemistry, Interscience Publishers, New York, 1956, p. 78.
[21] J. Dolinšek, S. Vrtnik, M. Klanjšek, Z. Jagličić, A. Smontara, I. Smiljanić, A. Bilušić, Y. Yokoyama, A. Inoue, C.V. Landauro, Phys. Rev. B 76 (2007) 054201.
[22] J. Dolinšek, P.J. McGuiness, M. Klanjšek, I. Smiljanić, A. Smontara, E.S. Zijlstra, S.K. Bose, I.R. Fisher, M.J. Kramer, P.C. Canfield, Phys. Rev. B 74 (2006) 134201.
[23] G. Trambly de Laissardière, J.-P. Julien, D. Mayou, Phys. Rev. Lett. 97 (2006) 026601.
[24] J. Dolinšek, P. Jeglič, M. Komelj, S. Vrtnik, A. Smontara, I. Smiljanić, A. Bilušić, J. Ivkov, D. Stanić, E.S. Zijlstra, B. Bauer, P. Gille, Phys. Rev. B 76 (2007) 174207.
[25] R. Kimmich, W. Unrath, G. Schnur, E. Rommel, J. Magn. Reson. 91 (1991) 136.
[26] T. Apih, V. Khare, M. Klanjšek, P. Jeglič, J. Dolinšek, Phys. Rev. B 68 (2003) 212202.
[27] T. Apih, M. Bobnar, J. Dolinšek, L. Jastrow, D. Zander, U. Köster, Solid State Commun. 134 (2005) 337.
[28] J. Dolinšek, T. Apih, M. Klanjšek, H.J. Kim, U. Köster, Catal. Today 120 (2007) 351.